






# Multilayer beamsplitter polarizers for key UV-FUV spectral lines of solar polarimetry

NURIA GUTIÉRREZ-LUNA,<sup>1,\*</sup>  GERARDO CAPOBIANCO,<sup>2</sup> ANDREA MARCO MALVEZZI,<sup>2,3</sup> CARLOS HONRADO-BENÍTEZ,<sup>1</sup> LUIS RODRÍGUEZ-DE MARCOS,<sup>1,4</sup>  JUAN I. LARRUQUERT,<sup>1</sup>  ANGELO GIGLIA,<sup>3</sup> NICOLA MAHNE,<sup>3</sup> STEFANO NANNARONE,<sup>3</sup> AND SILVANO FINESCHI<sup>2</sup>

<sup>1</sup>*GOLD-IO-CSIC Instituto de Óptica-Consejo Superior de Investigaciones Científicas, Madrid, Spain*

<sup>2</sup>*INAF - Osservatorio Astrofisico di Torino, Torino, Italy*

<sup>3</sup>*Istituto Officina dei Materiali -Consiglio Nazionale delle Ricerche, Trieste, Italy*

<sup>4</sup>*Catholic University of America and NASA Goddard Space Flight Center (CRESST II), Greenbelt, MD 20771, USA*

\*[nuria.gutierrez@csic.es](mailto:nuria.gutierrez@csic.es)

**Abstract:** Multilayer beamsplitter polarizers have been developed for improved solar polarimetry at key spectral lines. The advantage of beamsplitter polarizers is that a single device separates s from p polarization; this helps minimize attenuation and enables a more compact and lighter polarimeter, which is important for space instruments. Polarizers based on Al/AlF<sub>3</sub> multilayers were prepared for both C IV (155 nm) and Mg II (280 nm) lines, and based on Al/MgF<sub>2</sub> multilayers for H Lyman  $\alpha$  line (121.6 nm). Polarizers were designed to mainly reflect (transmit) s (p) polarization. Beamsplitter performance and throughput are shown to compare advantageously with polarizers in the literature. Beamsplitter polarizers kept a valuable performance after several years of ageing.

© 2022 Optica Publishing Group under the terms of the [Optica Open Access Publishing Agreement](#)

## 1. Introduction

The magnetic structure and thermodynamics of the solar corona and chromosphere have broad implications for solar/stellar atmospheres and they are essential research goals in solar physics and stellar astrophysics. These research fields require measuring the magnetic field in the chromosphere and solar corona.

The solar magnetic field is chiefly observed through light polarization. Line-radiation resonantly scattered by an anisotropic illuminating source is linearly polarized. In the presence of a magnetic field, this polarization is modified in direction and degree by the Hanle effect depending on the field's orientation and strength. The magnetic field diagnostics via the Hanle effect requires, therefore, to measure both the degree and direction of the polarization vector. The majority of the sensitive spectral lines to the magnetic field are localized at the ultraviolet (UV)-far UV (FUV) spectral ranges [1]. Therefore, UV-FUV polarimetry is a powerful tool that allows evaluating both effects and measuring the magnetic field [2]. Over the years, the scientific community has been proposing and developing space polarimeters designed to operate in the UV and FUV, such as the spectrometer-polarimeter of Intercosmos [3], UVSP of SolarMax [4], SUMER of SOHO [5], FUSP [6], LYOT of SMESE [7], CLASP [8], CLASP 2 [9], SUSP and CHROME instruments of SolmeX [10], and Polstar [11].

Hot astrophysical plasmas emit several UV and FUV spectral lines, particularly the H I Lyman-series, O VI, C IV, and Mg II lines. A key spectral line for solar atmosphere's polarimetry is H I Lyman  $\alpha$ , at 121.6 nm, which is the brightest line that is sensitive to Hanle effect [12,13,14,15].

Some studies show that a degree of polarization of up to 20% can be expected at the H-I Lyman- $\alpha$  line emitted in the solar corona [16,17]. C IV doublet, at 155 nm, is one of the most important transitions for optical diagnostics of hot plasmas in the interstellar and intergalactic media and stellar atmospheres [18]. Finally, the Mg II line is the most important radiator of the chromosphere [19,20,21]. Additionally, this resonance line is employed in determining bounds for temporal and/or spatial variations of the fine structure constant [18]. The Mg II spectral line is a tracer of the magnetic and thermal environment that spans from the photosphere to the upper chromosphere. Moreover, C IV and Mg II are two spectral lines of great importance in black-hole research [22].

A central element of polarimetry is linear polarizers. In addition to imaging instrumentation for astrophysics and solar physics, linear polarizers are used in many technological applications such as synchrotron radiation, lasers, ellipsometry, interferometry, atomic and molecular physics, particle-matter interaction, solid-state physics, magnetic and chiral-material analysis, etc.

Over the years, UV-FUV linear polarizers based on bulk transparent plates have been used, such as plate polarizers at Brewster angle [23] and piles of plates [24]. Other kinds of polarizers were based on mirror systems [25,26]. Regarding wire-grid polarizers, efficient reflective polarizers operating at 280 nm have been developed [27,28]; however, no wire-grid polarizer is currently available for a wavelength as short as 155 nm.

A multilayer coating is a choice of an efficient polarizer operating at a specific wavelength because it can be tuned at the desired wavelength(s) through layer thickness optimization. The first multilayer polarizer that reached a short FUV wavelength such as 121.6 nm was developed by Kim et al. [29]. Coating polarizers tuned at H I Lyman  $\alpha$  spectral line operating either by reflectance or by transmittance have been developed and reported [30,31,32,33].

A beamsplitter polarizer is a single optical element that splits the incoming beam that includes the two polarization components into two separated polarized beams. Bulk beamsplitter polarizers often consist of two prisms of a birefringent material with their bases in close contact, such as Wollaston and Rochon prisms. But these polarizers have small angular aperture along with relatively small deviation angles between the two components, so that long propagation distances are required, which may complicate the geometry of a space polarimeter or require extra folding optics. Commercial MgF<sub>2</sub> Wollaston and Rochon prisms have been found down to a wavelength of  $\sim$ 130 nm, and it might be difficult to extend them to the MgF<sub>2</sub> cutoff due to the decrease of MgF<sub>2</sub> birefringence at shorter wavelengths, which inverts sign at 119.4 nm [34], and to the need of hard-to-reach ultrasmooth polished surfaces to minimize absorption near the cut-off limit. Some drawbacks of these prisms are that they are bulky if a large aperture is required, and cannot operate at wavelengths as short as 121.6 nm. Transmission polarizers operating at 121.6 nm have been constructed by using pile-of-plates of LiF [35] and of MgF<sub>2</sub> [36]. In principle, the pile-of-plate could be used as a UV beamsplitter at 121.6 nm by using the reflected component of the first LiF or MgF<sub>2</sub> plate (e.g., Fineschi S, et al. [37]). However, the use of a pile-of-plate as an UV beamsplitter is not practical (e.g., large path difference between the transmitted and reflected beams), and no such device has ever been implemented.

Beamsplitter polarizers can also be made with coatings, so that film thicknesses are selected to provide the required reflective and transmissive profiles, and the angular separation between the beams can be made larger than with the above prisms; being a single device to separate the two crossed polarization components, multilayer beamsplitter polarizers are a useful tool that allows reducing energy losses and weight in a future more compact space polarimeter.

This research presents two types of multilayer beamsplitter polarizers tuned at key spectral lines for solar polarimetry, preferentially reflecting one polarization component and transmitting the other. Section 2 describes the experimental techniques used in this research. Section 3 presents polarizers based on Al/AlF<sub>3</sub> and on Al/MgF<sub>2</sub> multilayers (MLs) tuned at the pair C IV-Mg II spectral lines and at H I Lyman  $\alpha$  spectral line, respectively.

## 2. Experimental techniques

Multilayer beamsplitter polarizers were designed and prepared at GOLD (Spanish acronym of Thin Film Optics Group) in a 75-cm diameter, 100-cm height cylindrical stainless-steel chamber installed in an ISO-6 cleanroom dedicated to coat space optics. This chamber is pumped with a Velco250A cryopump, and the roughing pump is oil-free. Beamsplitter polarizers were deposited by thermal evaporation on substrates at room temperature. Polarizers tuned at 155 nm and 280 nm were prepared by depositing an  $(\text{Al}/\text{AlF}_3)_3$  multilayer on a quartz substrate. Polarizers tuned at 121.6 nm were prepared by depositing an  $(\text{Al}/\text{MgF}_2)_2$  multilayer on an  $\text{MgF}_2$  substrate. Quartz and  $\text{MgF}_2$  substrates were c-cut, i.e., with the optic axis (the only direction in a uniaxial crystal such as  $\text{MgF}_2$  and quartz in which a transmitted ray suffers no birefringence) perpendicular to the surface. 99.999% pure Al was deposited using a tungsten filament source. 99.99% purity  $\text{AlF}_3$  and VUV-grade  $\text{MgF}_2$  were evaporated using tungsten boats. The source-to-substrate distance was 68 cm. In-situ film thickness was measured with a quartz-crystal-monitor, which was previously calibrated by stylus profilometry.

Reflectance and transmittance with s and p polarization were measured at BEAR beamline of Elettra synchrotron [38]. Bending-magnet light source has polarization properties that depend on the emission angle. Fig. 1 bottom depicts how radiation is emitted in the vertical plane as a function of the photon energy. The radiation emitted by a synchrotron bending source can be modeled, by first principles, as the superposition of two linearly polarized fields (*modes*) out of phase of  $\pm 90^\circ$  oscillating in the plane normal to the field propagation direction. They are reported as vertical and horizontal components according to the fact that they are polarized along the normal to the orbit plane (the *vertical* component) and along the radius of curvature of the orbit (the *horizontal* component), respectively. The amplitudes of the components depend in value and sign on the positive/negative value of the angle of observation (the *take-off angle*) with respect to the orbit plane. The vertical component vanishes when the direction of observation is contained in the plane of the orbit (changing sign for angles of observation positive or negative with respect to orbit plane) while the horizontal component, which is symmetric in angle with respect to the orbit plane, assumes its maximum value for direction of observation parallel to the orbit plane. The vanishing of the vertical component and the simultaneous maximization of the horizontal one for observation along directions contained in the orbit plane is what is exploited in the present experiment (see also the caption of Fig. 1) for the preparation of a linearly polarized impinging field. Consequently, radiation is linearly polarized in the storage ring plane and elliptically polarized outside. Through a polarization selector, see Fig. 1, we regulate the polarization state of the light by selecting the appropriate emission angle. The selector consists of a double-slit device (see Fig. 1) that can be regulated to define the drop acceptance of the bending magnet source in the vertical direction (perpendicular to the ring plane). Almost full linearly polarized radiation is achieved by selecting the central portion of the bending magnet emission. Fig. 1 depicts how the central portion of the beam is selected.

All the campaigns of measurements have been done using a rigid setup based on detector and sample rotating  $90^\circ$  around the beam axis to cover the two polarization geometries without changing the relative sample-detector position. Fig. 2 shows the two geometries  $\sigma$  and  $\pi$ , where scattering plane is perpendicular and parallel, respectively, to the orbit plane. The figure shows the setup used for reflectivity; transmittance setup was accomplished by simply rotating the sample and the detector in the scattering plane.

All measurement campaigns to evaluate the stability of the polarizer tuned at 121.6 nm were carried out using a vertical acceptance semi-angle of 0.3 mrad. Regarding measurements of the polarizer tuned at 155 nm and 280 nm they were carried out with an acceptance semi-angle of 0.5 mrad, since radiation intensity was smaller compared with 121.6 nm. Since the accepted emission angle is not completely negligible, incoming light was not fully polarized.

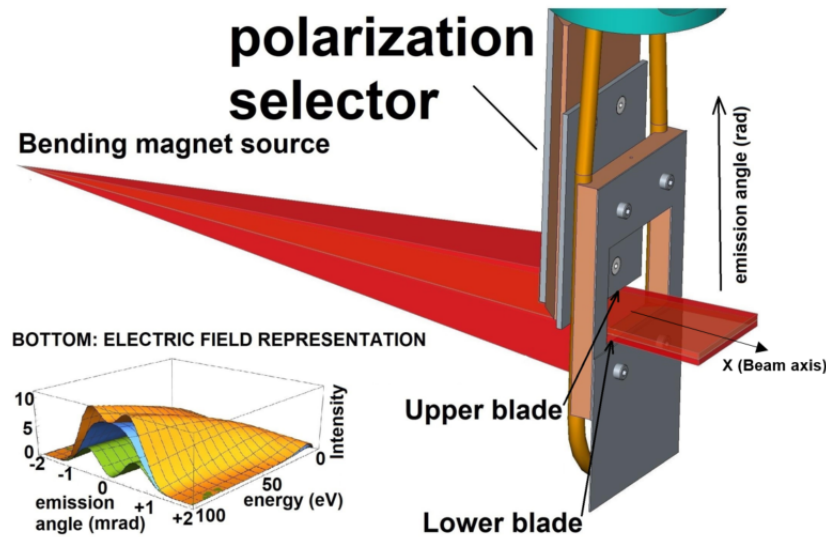


**Fig. 1.** Sketch of the polarization selector and of bending magnet source (bottom inset). The polarization selector is based on two blades moving along the vertical axis to define the polarization state of the light. The red cone represents the light emitted from synchrotron source. Linearly polarized light is selected by setting the two blades centered with respect to the synchrotron orbit. Bottom: longitudinal (blue surface) and perpendicular (green surface) modes of synchrotron radiation from 0 to 100 eV.

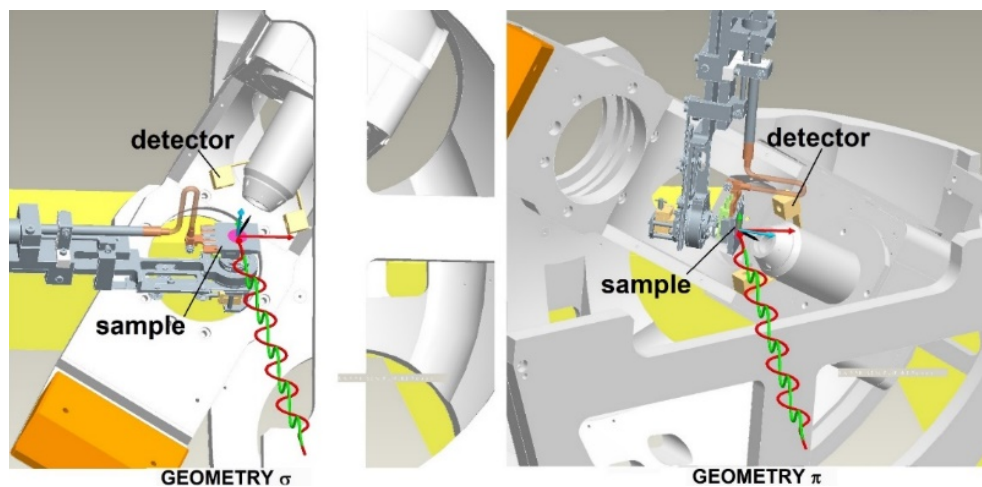


**Fig. 2.** Layout of  $\sigma$  and  $\pi$  geometries. In the  $\sigma$  geometry the scattering plane is perpendicular to orbit plane, in the  $\pi$  geometry the scattering plane is parallel.

The degree of linear polarization of the incoming beam with respect to the plane of incidence of the light beam impinging on the polarizer can be quantified through the relation  $f = ((I_s - I_p)/(I_s + I_p))$ ,  $s$  and  $p$  denote the intensity of the incident beam with the electric field perpendicular and parallel to the plane of incidence, respectively. The degree of polarization of the incoming light for the two acceptance angles has been determined by using as reference sample a  $\text{CaF}_2$  prism with the back side tilted of  $30^\circ$  with respect to the front surface, to avoid back reflectance effects, and by measuring the reflectance at the Brewster angle. The fitting of reflectivity data as a function of the rotation angle allowed determining the degree of linear polarization which is plotted in Table 1.

**Table 1. Degree of linear polarization used in the different wavelengths measurements**

Wavelength (nm)	Acceptance	f (degree of linear polarization)
276	$\pm 0.5$ mrad	0.92
191	$\pm 0.5$ mrad	0.90
146	$\pm 0.5$ mrad	0.90
121.6	$\pm 0.3$ mrad	0.95

Since the incoming light was not fully polarized, the measured reflectance and transmittance of the multilayer beamsplitter polarizer need to be corrected to obtain the real  $R_s$ ,  $T_s$  and  $R_p$ ,  $T_p$  (polarizer reflectance and transmittance with  $s$  or  $p$  polarization) by deducing the contribution of the crossed polarization. Here we adopted the terms  $R_\sigma$ ,  $T_\sigma$  and  $R_\pi$ ,  $T_\pi$  for the experimental measurements, where  $\sigma$  and  $\pi$  refer to the geometries with the incidence plane perpendicular and parallel, respectively, to the orbit plane, and  $R_s$ ,  $T_s$  and  $R_p$ ,  $T_p$  for the corrected quantities obtained by discounting the contribution of the crossed polarization present in  $R_\sigma$ ,  $T_\sigma$ ,  $R_\pi$ , and  $T_\pi$ . The full reflectance of a mirror, which adds the  $s$  and  $p$  contributions, is given by [39]:

$$R = \frac{R_s(1+f) + R_p(1-f)}{2} \quad (1)$$

Hence  $R_\sigma$  and  $R_\pi$  are obtained with Eq. 1 by using  $f$  ( $R_\sigma$ ) or  $-f$  ( $R_\pi$ ), since the chamber was rotated  $90^\circ$  between the two measurements, so that  $s$  turns  $p$  and  $p$  turns  $s$  after the rotation:

$$R_\sigma = \frac{R_s(1+f) + R_p(1-f)}{2} \quad (2)$$

$$R_\pi = \frac{R_s(1-f) + R_p(1+f)}{2} \quad (3)$$

Transmittance is given by Eqs. analogous to 1 to 3. By inverting Eqs. (2) and (3) one calculates the  $s$  and  $p$  terms from the  $\sigma$  and  $\pi$  measurements:

$$R_s = \frac{(R_\sigma - R_\pi) + f(R_\sigma + R_\pi)}{2f} \quad (4)$$

$$R_p = \frac{f(R_\pi + R_\sigma) + (R_\pi - R_\sigma)}{2f} \quad (5)$$

$$T_s = \frac{(T_\sigma - T_\pi) + f(T_\sigma + T_\pi)}{2f} \quad (6)$$

$$T_p = \frac{f(T_\pi + T_\sigma) + (T_\pi - T_\sigma)}{2f} \quad (7)$$

For linearly polarized light ( $f = 1$ ),  $R_s$ ,  $T_s$ ,  $R_p$ , and  $T_p$  are obviously coincident with  $R_\sigma$ ,  $T_\sigma$ ,  $R_\pi$ , and  $T_\pi$ , respectively.



For both transmittance and reflectance measurements, the beam impinged on the sample from the coating side. The light spot cross-section at the focus position was set at  $400 \times 400 \mu\text{m}$  horizontal  $\times$  vertical, with a divergence of 20 mrad, and the width spectral purity  $\Delta E/E = 10^{-2}$ . The incident flux was  $\sim 10^9$  photons/s. Transmittance and reflectance were obtained by averaging at each photon energy a set of light and dark measurements (eventually subtracted). The lowest measurable flux (both in transmission and reflection) was  $\sim 10^6$  photons/s with detection dynamics of three digits. The angles of incidence for reflected or transmitted light were set with an accuracy of  $\sim 0.1^\circ$ . A silicon diode (IRD-AXUV100) was used as a radiation detector. DC Measurements were taken by a picoammeter. The intensity of the incident flux was monitored by measuring the refocusing mirror drain current with a second picoammeter.

Samples were stored in a desiccator with 20% relative humidity during the ageing period.

### 3. Results

#### 3.1. Multilayer beamsplitter polarizer tuned at 155 nm and 280 nm

The multilayer beamsplitter polarizer was designed to preferentially reflect the s component and transmit the p component of the incoming light and it was designed to operate at an angle of incidence of  $70^\circ$ . Fig. 3 displays the experimental reflectance and transmittance measured in the two planes mentioned in Section 2 of an  $(\text{Al}/\text{AlF}_3)_3$  multilayer beamsplitter polarizer tuned at 155 and 280 nm. The polarizer was characterized at  $70^\circ \pm 5^\circ$ . Fig. 4 displays the corrected reflectance and transmittance for s and p polarization obtained from data plotted in Fig. 3 by applying Eqs. 4 to 7. Measurements correspond to samples aged of 3 years.

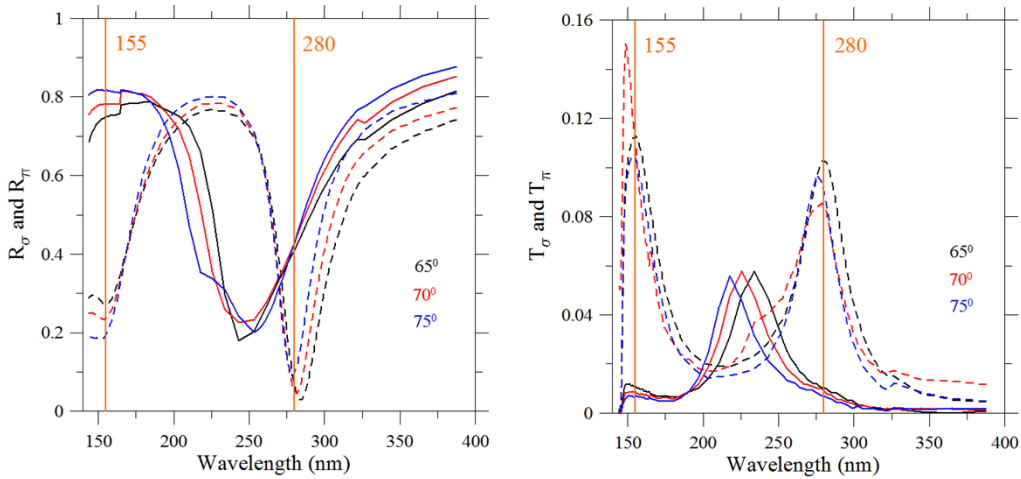


**Fig. 3.** Reflectance (left) and transmittance (right) at three incidence angles of a beamsplitter polarizer tuned at 155 and 280 nm aged of 3 years.  $R_\sigma$ ,  $R_\pi$ ,  $T_\sigma$ , and  $T_\pi$  stand for experimental reflectance/transmittance measurements before deducting the contribution of the cross polarization. Solid line:  $\sigma$ ; dashed line:  $\pi$ .

We used two parameters to evaluate polarizer quality: the modulation factor  $\mu$  and the figure of merit  $\kappa$  [37,40]:

$$\mu_R = \frac{R_s - R_p}{R_s + R_p} \quad \mu_T = \frac{T_p - T_s}{T_p + T_s} \quad (8)$$

$$\kappa_R = \mu_R \sqrt{R} \quad \kappa_T = \mu_T \sqrt{T} \quad (9)$$

$\mu$  describes the ability of a polarizer to polarize by reflection or transmission, and  $\kappa$  is the product of  $\mu$  times the square root of the reflectance or transmittance averaged over the two polarizations

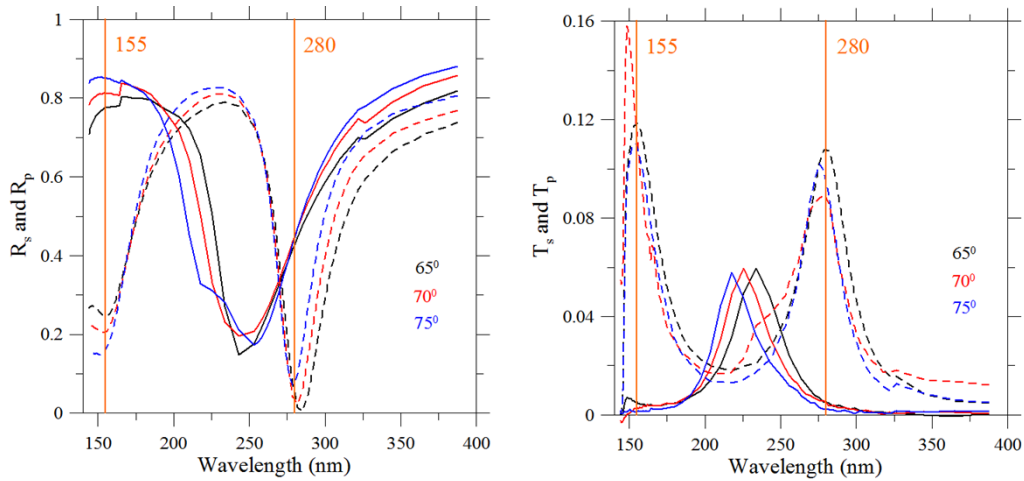


**Fig. 4.** Reflectance (left) and transmittance (right) at three incidence angles ( $65^\circ$ ,  $70^\circ$ ,  $75^\circ$ ) of a multilayer beamsplitter polarizer aged for 3 years.  $R_s$ ,  $R_p$ ,  $T_s$ , and  $T_p$  stand for reflectance/transmittance measurements corrected to remove the estimated crossed polarization component of the incident beam using Eqs. 4 to 7. Solid line: s; and dashed line: p.

$R = 0.5(R_s + R_p)$ , and the same with  $T$ . Therefore, this “quality factor” evaluates the ideality of the polarizer, so that we evaluated polarizer efficiency through  $\kappa$ . The above definitions of  $\mu$  assume that it is simpler to obtain  $R_s > R_p$  and  $T_s < T_p$  than the opposite. The optimum value of  $\mu_R$  and  $\mu_T$  is +1, which corresponds to  $R_p = 0$  and  $T_s = 0$ , respectively.  $\kappa$  provides information about the trade-off between polarization efficiency and throughput. The maximum theoretical value of  $\kappa$  is  $2^{-1/2} = 0.707$ , corresponding to  $\mu = 1$  and  $R = 0.5$  or  $T = 0.5$ . Fig. 5 displays  $\mu$  and  $\kappa$  for reflectance and transmittance measurements plotted in Fig. 4. Table 2 summarizes  $\mu$  and  $\kappa$  at the three incidence angles and at the two spectral lines.

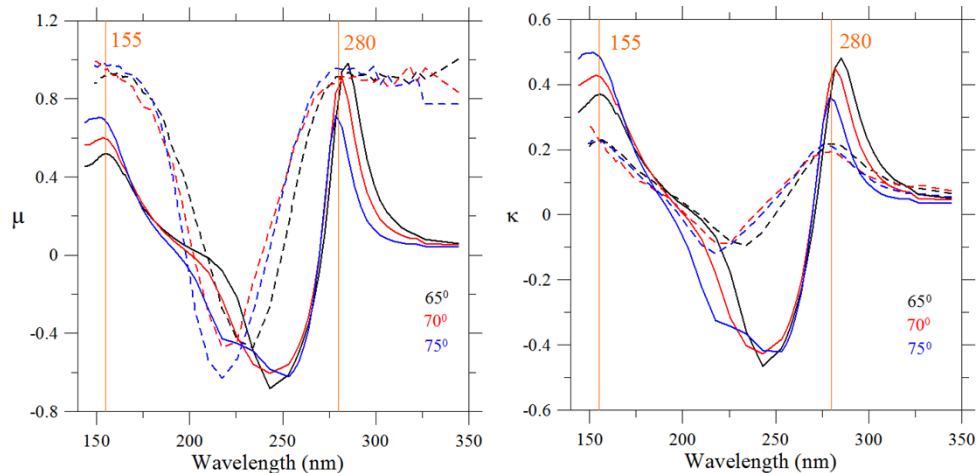


**Fig. 5.** Modulation factor,  $\mu$  (left), and figure of merit,  $\kappa$  (right), at various incidence angles of the multilayer beamsplitter polarizer plotted in Fig. 4. The solid and dashed lines correspond to reflectance and transmittance values, respectively.

**Table 2.**  $\mu$  and  $\kappa$  at the indicated wavelengths and angles of incidence for the multilayer beamsplitter polarizers presented in Figs. 5 and 10

Angle	@155 nm				@280 nm				@121.6 nm			
	$\mu_R$	$\kappa_R$	$\mu_T$	$\kappa_T$	$\mu_R$	$\kappa_R$	$\mu_T$	$\kappa_T$	$\mu_R$	$\kappa_R$	$\mu_T$	$\kappa_T$
65°	0.516	0.369	0.913	0.227	0.816	0.398	0.912	0.216				
70°	0.596	0.425	0.946	0.230	0.868	0.427	0.899	0.193	0.937	0.602	0.929	0.281
75°	0.683	0.486	0.975	0.230	0.685	0.354	0.952	0.209	0.823	0.529	0.767	0.252

Preliminary data of a beamsplitter polarizer based on an Al/AlF<sub>3</sub> ML tuned at C IV and Mg II spectral lines had been designed and prepared by the present research team [41]. However, although most evaluation parameters were rather satisfactory for that previous beamsplitter polarizer, there was hardly any difference between  $R_s$  and  $R_p$  at 280 nm. In the present work, the ML design was finely tuned to satisfy all four requirements on  $R_s$ ,  $R_p$ ,  $T_s$ , and  $T_p$  both at 155 and 280 nm.

### 3.2. Multilayer beamsplitter polarizer tuned at 121.6 nm

Beamsplitter polarizers based on Al/MgF<sub>2</sub> were designed to optimize its polarization properties at 121.6 nm to operate at an angle of incidence of 70°. Figs. 6 and 8 display the experimental reflectance and transmittance measurements of a beamsplitter polarizer at angles of incidence of 70° and 75°, respectively. Measurements correspond to samples both fresh, and after 1 and 4 years of ageing. Figs. 7 and 9 display s and p polarization reflectance and transmittance obtained from data plotted in Figs. 6 and 8, respectively, by applying Eqs. 4 to 7. Measurements correspond to samples both fresh and after 1 and 4 years of ageing. Fig. 10 displays  $\mu$  and  $\kappa$  for the multilayer beamsplitter polarizer plotted in Figs. 7 and 9. Table 2 displays  $\mu$  and  $\kappa$  of this polarizer at 121.6 nm. Preliminary data of the present polarizer measured for the fresh polarizer and at a single incidence angle had been published in [41].

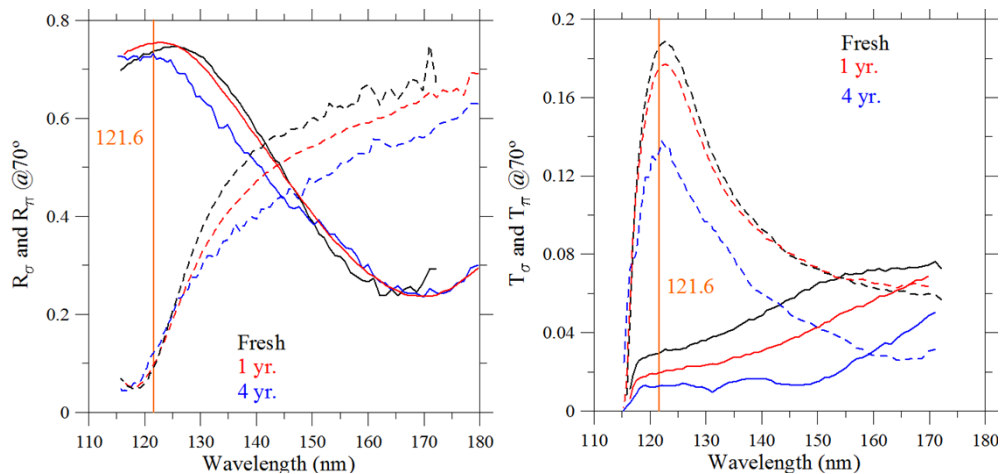


**Fig. 6.** Reflectance (left) and transmittance (right) at 70° of a multilayer beamsplitter polarizer optimized at 121.6 nm for fresh sample and for the sample aged of one and four years.  $R_\sigma$ ,  $R_\pi$ ,  $T_\sigma$ , and  $T_\pi$  stand for experimental reflectance/transmittance measurements before deducting the contribution of the cross polarization. Solid line:  $\sigma$ ; dashed line:  $\pi$ .



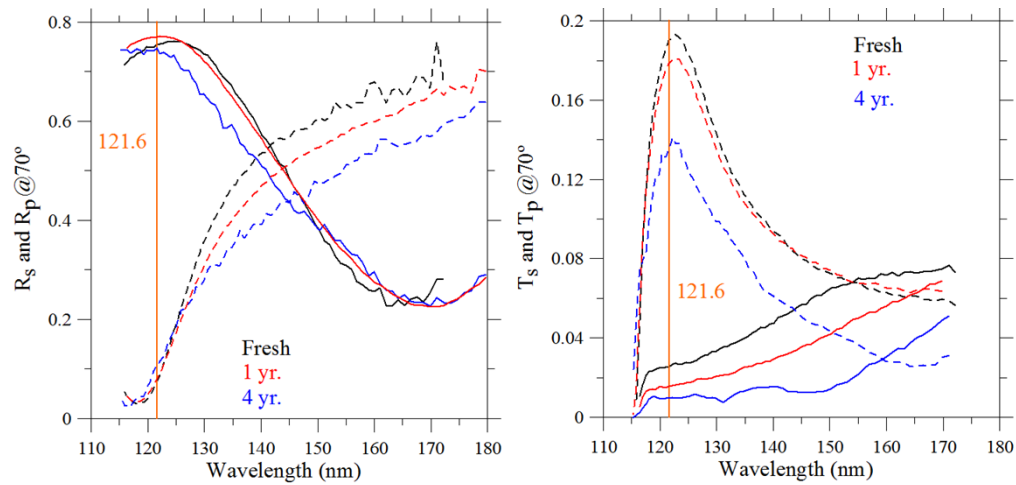


**Fig. 7.** Reflectance (left) and transmittance (right) at  $70^\circ$  of a multilayer beamsplitter polarizer optimized at 121.6 nm for the fresh sample and for the sample aged one and four years.  $R_s$ ,  $R_p$ ,  $T_s$ , and  $T_p$  stand for reflectance/transmittance measurements corrected to remove the estimated crossed polarization component of the incident beam using Eqs. 4 to 7. Solid line: s; dashed line: p.

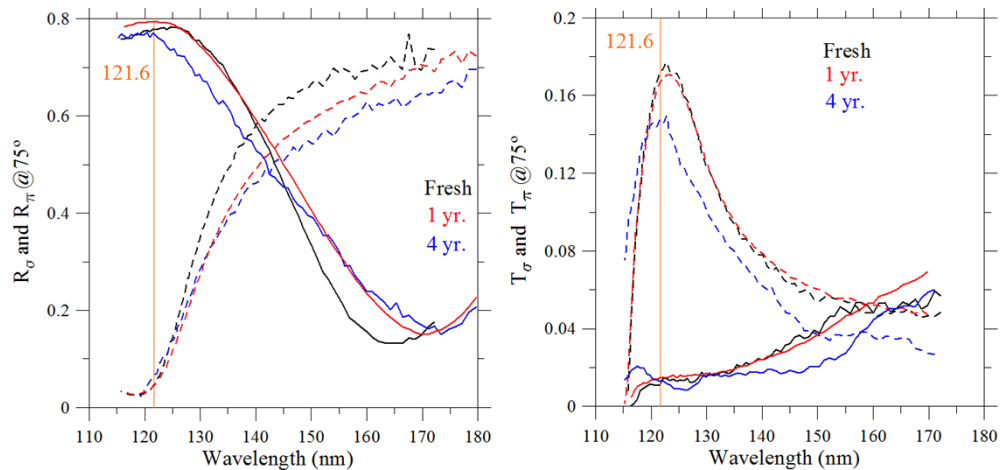


**Fig. 8.** Reflectance (left) and transmittance (right) at  $75^\circ$  of a multilayer beamsplitter polarizer optimized at 121.6 nm for fresh sample and for the sample aged one and four years.  $R_\sigma$ ,  $R_\pi$ ,  $T_\sigma$ , and  $T_\pi$  stand for experimental reflectance/transmittance measurements before deducting the contribution of the cross polarization. Solid line:  $\sigma$ ; dashed line:  $\pi$ .

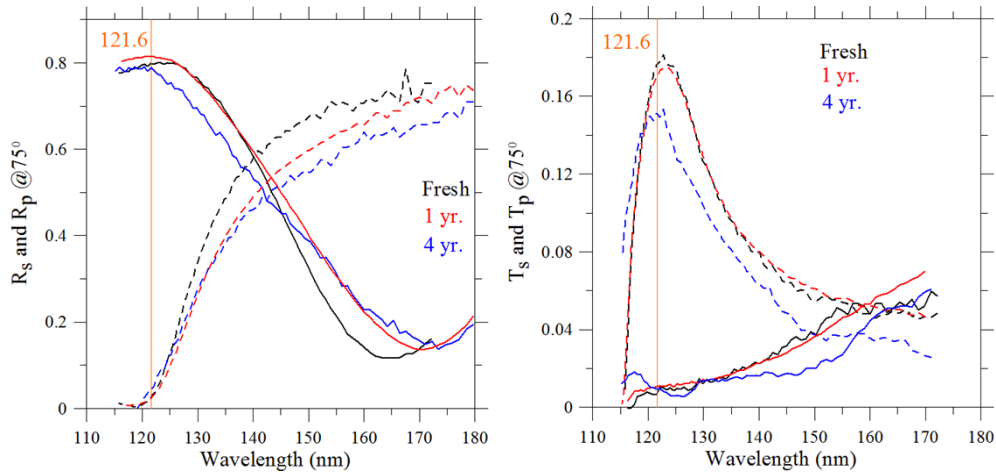


**Fig. 9.** Reflectance (left) and transmittance (right) at 75° of a multilayer beamsplitter polarizer optimized at 121.6 nm for the fresh sample and for the sample aged one and four years.  $R_s$ ,  $R_p$ ,  $T_s$ , and  $T_p$  stand for reflectance/ transmittance measurements corrected to remove the estimated crossed polarization component of the incident beam using Eqs. 4 to 7. Solid line: s; dashed line: p.

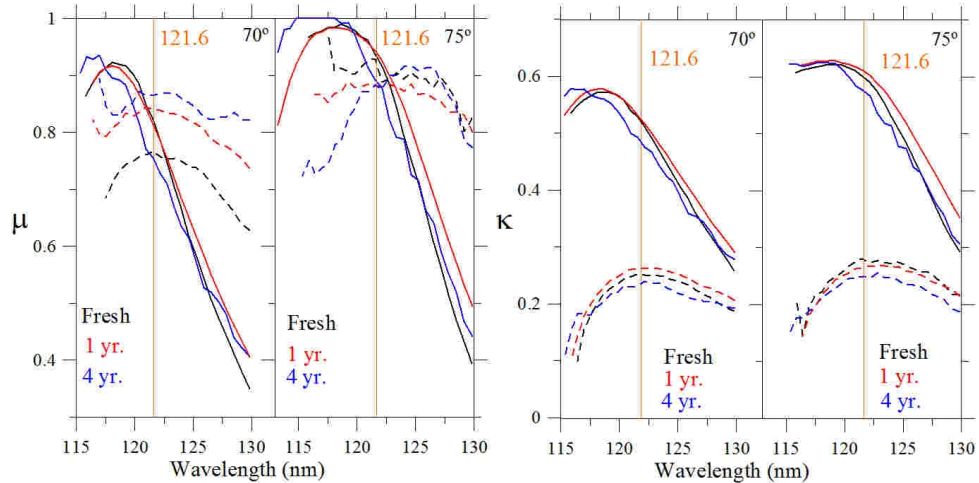


**Fig. 10.**  $\mu$  (left) and  $\kappa$  (right) at the indicated angles of the multilayer beamsplitter polarizer optimized at 121.6 nm calculated from data plotted in Figs. 7 and 9. The solid and dashed lines correspond to reflectance and transmittance values, respectively. Measurements for the fresh sample and for the sample aged one and four years are shown.

#### 4. Discussions

The polarizers presented in Section 3 display remarkable polarization properties at the target spectral lines both in reflectance and in transmittance. The polarizers designed at 155 and 280 nm can operate in a range of incidence angles between 65° and 75°. The polarizer designed at 121.6 nm presents a high polarization contrast at angles of incidence of 70° and 75°, which might be somewhat extended to a wider angle range. Regarding the latter polarizer, we note that  $\mu_R$  and  $\mu_T$  are similar, which means that the polarizer has the same capacity for preferentially reflecting one polarization component and for preferentially transmitting the other component, even though  $\kappa$  is larger when operating by reflectance.

The usefulness of the present beamsplitters can be evaluated by comparison with more conventional polarizers. Table 3 compares the quality parameters of the present multilayer beamsplitter polarizers with calculated data of a parallel plate of MgF<sub>2</sub> or quartz at Brewster angle, a LiF pile of plates, and a (MgF<sub>2</sub>/Al)<sub>2</sub> coating polarizer solely operating by reflection [30]. Even though  $\mu_R$  approaches 1 for plates at Brewster angle, the present multilayer beamsplitter polarizers provide considerably larger  $\kappa_R$ , which is combined with larger  $\mu_T$  and  $\kappa_T$ .

**Table 3. Comparison between the present multilayer beamsplitter polarizers shown in Figs. 5 (for a 3-year aged multilayer beamsplitter tuned at 155 and 280nm and aged at 70° and 75°) and Fig. 10 (for the multilayer beamsplitter tuned at 121.6nm and aged one year at 70° and 75°), a parallel plate of MgF<sub>2</sub> at Brewster angle (BA), a LiF pile of plates at BA, a (MgF<sub>2</sub>/Al)<sub>2</sub> coating polarizer at 66° only operating by reflectance, and a parallel plate of quartz at BA**

		155 nm				280 nm				121.6 nm			
		$\mu_R$	$\kappa_R$	$\mu_T$	$\kappa_T$	$\mu_R$	$\kappa_R$	$\mu_T$	$\kappa_T$	$\mu_R$	$\kappa_R$	$\mu_T$	$\kappa_T$
ML Beamsplitter	70°	0.596	0.425	0.946	0.230	0.869	0.428	0.899	0.193	0.814	0.531	0.839	0.262
	75°	0.683	0.486	0.975	0.230	0.685	0.354	0.952	0.209	0.943	0.610	0.881	0.265
MgF <sub>2</sub> plate (BA) <sup>a</sup>		~1	0.263	0.074	0.072	~1	0.238	0.061	0.058	~1	0.251	0.067	0.065
LiF pile of plates (BA) <sup>b</sup>	4 plates									0.992	0.505	0.67	0.235
	6 plates									0.986	0.488	0.80	0.179
(MgF <sub>2</sub> /Al) <sub>2</sub> <sup>c</sup>										0.92	0.55	-	-
Quartz plate (BA) <sup>a</sup>		0.996	0.366	0.156	0.145	0.996	0.316	0.112	0.106				

<sup>a</sup>For parallel plates, calculations were performed at the Brewster angle of the corresponding material at the indicated wavelengths. For plates at 155/280 nm calculations were performed at an angle averaged over the Brewster angles at the two wavelengths.

<sup>b</sup>W.C. Walker [35]. For the pile of plates,  $\mu_R$  and  $\kappa_R$  was calculated with the optical constants of LiF [42].

<sup>c</sup>Cfr. Table 2 in Bridou et al. [30].

The beamsplitter polarizers developed both for the pair 155/280 nm and for 121.6 nm spectral lines have a larger  $\kappa$  for reflectance than for transmittance; this is due to the fact that the transmitted polarization component is attenuated by the total Al thickness. Even though this could be improved by using thinner Al layers, ultrathin continuous layers deposited by evaporation may have limited reproducibility. Such more transparent polarizers are proposed as continuation research. In contrast, the presence of Al films in the polarizer involves some filtering properties, so that longer wavelengths than the target lines are more strongly absorbed. This is so partly because Al absorption coefficient increases with wavelength [43] and partly because the interference at the multilayer results in a higher average s + p transmittance at the target line than away. This property could partly compensate for the lower throughput of the polarizers by transmittance compared to reflectance.

The presented multilayer beamsplitter polarizers present unique properties: i) high polarization contrast in a wide range of incidence angles, which is an important advantage compared to other solutions such as Rochon prisms, with smaller acceptance angles; ii) they can be cost-effectively applied over large aperture optics, contrarily to the difficulty, cost, and size of large-aperture

Rochon polarizers; iii) when operating by transmission, they reject the NUV-VIS-NIR, so that these polarizers, when operating by transmission, can be useful for applications in which heat is a problem, for instance, in direct solar observations.

## 5. Conclusions

Multilayer beamsplitter polarizers tuned at key UV and FUV spectral lines for solar physics applications have been developed. These polarizers were designed to preferentially reflect (transmit) s (p) polarization at the spectral lines of C IV (155 nm) and Mg II (280 nm) or at H I Lyman  $\alpha$  line (121.6 nm). Polarizer performance was evaluated in terms of the modulation factor and the figure of merit  $\kappa$  which includes throughput. Beamsplitter polarizers demonstrated better throughput than a parallel plate or a pile of plates operating at Brewster angle. Coating polarizers also involve a wider acceptance angle than Rochon polarizers and are more cost-effective for large optics. When they operate by transmission, they also provide VIS-NIR filtering. The polarizers optimized at the two optical profiles kept valuable performance at the target wavelengths after a long period of ageing, which is a critical requirement for optical devices intended to operate in space polarimeters. Future space polarimeters can benefit from the present beamsplitter polarizers with a gain in performance, a lighter instrument, and more compact geometry.

**Funding.** Ministerio de Ciencia e Innovación (PID2019-105156GB-I00 and ESP2016-76591-P); National Programme for Research, Subdirección General de Proyectos de Investigación. The research leading to this result has been supported by the project CALIPSOplus under Grant Agreement 730872 from the EU Framework Programme for Research and Innovation HORIZON 2020.

**Acknowledgments.** We acknowledge support by the European Community-Research Infrastructure Action under the FP6 'Structuring the European Research Area' Programme (through the Integrated Infrastructure Initiative 'Integrating Activity on Synchrotron and Free Electron Laser Science'); measurements were performed under Elettra proposal numbers 20150344, 20155497, 20165506, 20170445, 20180233, 20190371, 20210186 and AHEAD2020 proposal 871158. LRM acknowledges CRESST II cooperative agreement supported by NASA under award number 80GSFC21M0002. We acknowledge support by "Subdirección General de Proyectos de Investigación, Ministerio de Ciencia e Innovación", projects number ESP2016-76591-P and PID2019-105156GB-I00.

**Disclosures.** The authors declare no conflict of interest.

**Data availability.** Data corresponding to the results shown in this paper is not available publicly but may be obtained from the authors upon reasonable request.

## References

1. A. I Gómez de Castro, P. Sestito, N. Sánchez, F. López-Martínez, J. Seijas, M. Gómez, P. Rodríguez, J. Quintana M. Ubierna, and J. Muñoz, "World Space Observatory-Ultraviolet: ISSIS, the imaging instrument," *Adv. Space Res.* **53**(6), 996–1002 (2013).
2. J. Hough, "Polarimetry: a powerful diagnostic tool in astronomy," *Astron. Geo.* **47**, 3.31–3.35 (2006).
3. J. O. Stenflo, D. Dravins, N. Whilborg, A. Bruns, V. K. Prokofev, I. A. Zhitnik, H. Biverot, and L. Stenmark, "Search for spectral line polarization in the solar vacuum ultraviolet," *Sol. Phys.* **66**, 13–20 (1980).
4. B. E. Woodgate, E. A. Tandberg-Hanssen, E. C. Bruner, J. M. Beckers, J. C. Brandt, W. Henze, C. L. Hyder, M. W. Kalet, P. J. Kenny, E. D. Knox, A. G. Michalitsianos, R. Rehse, R. A. Shine, and H. D. Tinsley, "The ultraviolet spectrometer and polarimeter on the solar maximum mission," *Sol. Phys.* **65**, 73–90 (1980).
5. N.-E. Raouafi, P. Lemaire, and S. Sahal-Bréchet, "Detection of the O VI 103.2 nm line polarization by the SUMER spectrometer on the SOHO spacecraft," *Astron. Astrophys.* **345**, 999–1005 (1999).
6. K. H. Nordsieck and W.M. Harris, "Ultraviolet astronomical polarimetry: some results and prospects," *Proc. SPIE* **3764**, 124 (1999).
7. J. C. Vial, F. Auchère, J. Chang, C. Fang, W. Q. Gan, K. L. Klein, J. Y. Prado, F. Rouesnel, A. Sémary, G. Trotted, and C. Wang, "SMESE (Small Explorer for Solar Eruptions): A microsatellite mission with combined solar payload," *Adv. Space Res.* **41**, 183 (2008).
8. R. Kano, T. Bando, N. Narukage, R. Ishikawa, S. Tsuneta, Y. Katsukawa, M. Kubo, S. Ishikawa, H. Hara, T. Shimizu, Y. Suematsu, K. Ichimoto, T. Sakao, M. Goto, Y. Kato, S. Imada, K. Kobayashi, T. Holloway, A. Winebarger, J. Cirtain, B. de Pontieu, R. Casini, J. Trujillo-Bueno, J. Stepan, R. Manso Sainz, L. Belluzzi, A. A. Ramos, F. Auchère, and M. Carlsson, "Chromospheric Lyman-Alpha Spectro-Polarimeter (CLASP)," *Proc. SPIE* **8443**, 84434F (2012).
9. N. Narukage, D. E. McKenszie, R. Ishikawa, J. Trujillo-Bueno, B. de Pontieu, M. Kubo, S. Ishikawa, R. Kano, Y. Suematsu, M. Yoshida, L. A. Rachmeler, K. Kobayashi, J. W. Cirtain, A. R. Winebarger, A. A. Ramos, T. del Pino

- Aleman, J. Stepan, L. Belluzzi, J. I. Larruquert, F. Auchère, J. Leenaarts, and M. J. L. Carson, "Chromospheric Layer SpectroPolarimeter (CLASP 2)," *Proc. SPIE* **9905**, 990508 (2016).
10. H. Peter, L. Abbo, V. Andretta, F. Auchère, A. Bemporad, F. Berrilli, V. Bommier, A. Braukhane, R. Casini, W. Curdt, J. Davila, H. Dittus, S. Fineschi, A. Fludra, A. Gandorfer, D. Griffin, B. Inhester, A. Lagg, E. Landi Deg'Innocenti, V. Maiwald, R. Manso Sainz, V. Martínez Pillet, S. Matthews, D. Moses, S. Parenti, A. Pietarila, D. Quantius, N. E. Raouafi, J. Raymond, P. Rochus, O. Romberg, M. Schlotterer, U. Schüle, S. Solanki, D. Spadaro, L. Teriaca, S. Tomczyk, J. Trujillo-Bueno, and J. C. Vial, "Solar magnetism eXplorer (SolmeX)," *Exp. Astron.* **33**, 271–303 (2012).
  11. P. A. Scowen, K. Gayley, C. Neiner, G. Vasudevan, R. Woodruff, R. Ignace, R. Casini, T. Hull, A. Nordt, and H. P. Stahl, "The PolStar High Resolution Spectropolarimetry MIDEEX Mission," *Proc. SPIE* **11819**, 1181908 (2021).
  12. S. Fineschi, "Space-based Instrumentation for Magnetic Field Studies of Solar and Stellar Atmospheres," *ASP Conf. Ser.* **248**, 597–605 (2001).
  13. V. Bommier, "Hanle effect from a dipolar magnetic structure: the case of the solar corona and the case of a star," *Astron. Astrophys.* **539**, A122 (2012).
  14. S. Fineschi, R. B. Hoover, and A. B. C. Walker II, "Hydrogen Lyman- $\alpha$  coronagraph/polarimeter," *Proc. SPIE* **1546**, 402–413 (1991).
  15. J. Trujillo Bueno, J. Stepán, and R. Casini, "The Hanle effect of the Hydrogen Ly $\alpha$  line for probing the magnetism of the solar transition region," *ApJL* **738**, L11 (2011).
  16. V. Bommier and S. Sahal-Bréchet, "The Hanle effect of the coronal L $\alpha$  line of hydrogen: Theoretical investigation," *Sol. Phys.* **78**, 157–178 (1982).
  17. S. Fineschi, R. B. Hoover, J. M. Fontenla, and A. B. C. Walker II, "Polarimetry of extreme ultraviolet lines in solar astronomy," *Opt. Eng.* **30**, 1161–1168 (1991).
  18. U. Griesmann and R. Kling, "Interferometric measurement of resonance transition wavelengths in C IV, Si IV, Al III, Al II, and Si II," *ApJ* **536**(2), 1 (2000).
  19. J. B. Gurman, "The MG II h line in sunspot umbrae," *Sol. Phys.* **90**, 13–15 (1984).
  20. W. Henze Jr. and J. O. Stenflo, "Polarimetry in the MgII h and k Lines," *Sol. Phys.* **111**, pp. 243–254 (1987).
  21. Luca Belluzzi and Javier Trujillo Bueno, "The polarization of the solar Mg II h and k lines," *ApJL* **750**, L11 (2012).
  22. L. C. Popović, "Broad spectral lines in AGNs and supermassive black hole mass measurements," *Open Astron.* **29**, 1–14 (2020).
  23. F. Bridou, M. Cuniot-Ponsard, J. M. Desvignes, M. Richter, U. Kroth, and A. Gottwald, "Experimental determination of optical constants of MgF<sub>2</sub> and AlF<sub>3</sub> thin films in the vacuum ultra-violet wavelength region (60–124 nm), and its application to optical designs," *Opt. Commun.* **283**, 1351–1358 (2010).
  24. M. Keim, A. Werner, D. Hasselkamp, D. H. Schartner, H. J. Lüdde, A. Achenbach, and T. Kirchner, "Lyman- $\alpha$  line polarization after proton impact on atomic hydrogen," *J. Phys. B: At. Mol. Opt. Phys.* **38**, 4045–4055 (2005).
  25. M. Yang, C. Cobet, C. Werner, and N. Esser, "Optical polarizer integrated with suppression of higher harmonics in the vacuum ultraviolet and soft X-Ray spectral regions," *App. Phys. Lett.* **92**, 011110 (2008).
  26. N. V. Smith and M. R. Howells, "Whispering galleries for the production of circularly polarized synchrotron radiation in the XUV region," *Nucl. Instrum. Methods Phys. Res. A* **347**, 115–118 (1994).
  27. T. Siefke, S. Kroker, K. Pfeiffer, O. Puffky, K. Dietrich, D. Franta, I. Ohlídal, A. Szeghalmi, E. B. Kley, and A. Tünnermann, "Materials Pushing the Application Limits of Wire Grid Polarizers further into the Deep Ultraviolet Spectral Range," *Adv. Optical Mater.* **4**, 1780–1786 (2016).
  28. L. Rodríguez de Marcos, O. B. Leong, T. C. Asmara, S. P. Heussler, M. B. H. Breese, and A. Rusydi, "Nanoscale dielectric grating polarizers tuned to 4.43 eV for ultraviolet polarimetry," *Opt. Express* **28**, 12936–12950 (2020).
  29. J. Kim, M. Zukic, and D. G. Torr, "Multilayer thin film design as far ultraviolet polarizers," *Proc. SPIE* **1742**, 413 (1992).
  30. F. Bridou, M. Cuniot-Ponsard, J. M. Desvignes, A. Gottwald, U. Kroth, and M. Richter, "Polarizing and non-polarizing mirrors for the hydrogen Lyman- $\alpha$  radiation at 121.6 nm," *Appl. Phys A* **102**, 641–649 (2011).
  31. J. I. Larruquert, A. M. Malvezzi, A. Giglia, J. A. Aznárez, L. V. Rodríguez-de Marcos, J. A. Méndez, P. Miotti, F. Frassetto, G. Massone, G. Capobianco, S. Fineschi, G. Crescenzo, and S. Nannarone, "Polarizers for a spectral range centered at 121.6 nm operating by reflectance or by transmittance," *Proc. SPIE* **9510**, 951008 (2015).
  32. J. I. Larruquert, A. M. Malvezzi, A. Giglia, J. A. Aznárez, L. V. Rodríguez-de Marcos, J. A. Méndez, P. Miotti, F. Frassetto, G. Massone, S. Nannarone, G. Crescenzo, G. Capobianco, and S. Fineschi, "Reflective and transmissive broadband coating polarizers in a spectral range centered at 121.6 nm," *J. Opt.* **16**, 125713 (2014).
  33. N. Narukage, M. Kubo, R. Ishikawa, S. N. Ishikawa, Y. Katsukawa, t. Kobiki, G. Giono, R. Kano, T. Bando, S. Tsuneta, F. Auchère, K. Kobayashi, A. Winebarger, J. McCandless, J. Chen, and J. Choi, "High reflective coating for Vacuum Ultraviolet Spectropolarimeter," *Sol. Phys.* **292**, 40 (2017).
  34. V. Chandrasekharan and H. Damany, "Anomalous dispersion of birefringence of sapphire and magnesium fluoride in the vacuum ultraviolet," *Appl. Opt.* **8**, 671–675 (1969).
  35. W. C. Walker, "Pile-Of-Plates Polarizer for the vacuum Ultraviolet," *App. Opt.* **3**, 1457–1459 (1964).
  36. H. Winter and H. W. Ortjohann, "High transmission polarization analyzer for Lyman- $\alpha$  radiation," *Rev. Sci. Instrum.* **58**(3), 359–362 (1987).
  37. S. Fineschi, L. D. Gardner, J. L. Kohl, M. Romoli, E. Pace, G. Corti, and G. Noci, "Polarimetry of the UV solar corona with ASCE," *Proc. SPIE* 3764, 147–160 (1999).
  38. <https://www.elettra.trieste.it/lightsources/elettra/elettra-beamlines/bear/beamline-description/page-7.html>

39. J. I. Larruquert, J. A. Méndez, and J. A. Aznárez, "Far-ultraviolet reflectance measurements and optical constants of unoxidized aluminum films," *Appl. Opt.* **34**, 4892–4899 (1995).
40. O. Ivanova, S. Pasini, M. Mokenbusch, and O. Holderer, "Instrument developments and recent scientific highlights at the J-NSE," *J. Phys.: Conf. Ser.* **862**, 012009 (2017).
41. J. I. Larruquert, A. Malvezzi, L. R. de Marcos, A. Giglia, N. Gutiérrez-Luna, L. Espinosa-Yañez, C. Honrado-Benítez, J. A. Aznárez, G. Massone, G. Capobianco, S. Fineschi, and S. Nannarone, "Polarizers tuned at key far-UV spectral lines for space instrumentation," *Proc. SPIE* **10235**, 102350K–1 (2017).
42. E. D. Palik and W.R. Hunter, "Lithium Fluoride," in *Handbook of optical constants of solids* (Academic Press, 1997).
43. E. Shiles, T. Sasaki, M. Inokuti, and D. Y. Smith, "Self-consistency and sum-rule test in the Kramers-Kronig analysis of optical data: Application to aluminium," *Phys. Rev. B* **22**, 1612 (1980).